Chemical and Structural Properties of a Whitlockite-like Phosphate, $Ca_9FeD(PO_4)_7$

A. A. Belik,[†,||] F. Izumi,*[,†] S. Yu. Stefanovich,[‡] B. I. Lazoryak,[‡] and K. Oikawa[§]

Advanced Materials Laboratory, National Institute for Materials Science, 1-1 Namiki, Tsukuba, Ibaraki 305-0044, Japan, Department of Chemistry, Moscow State University, Leninsky Gory, Moscow 119899, Russia, and Institute of Materials Structure Science, High Energy Accelerator Research Organization, 1-1 Oho, Tsukuba, Ibaraki 305-0801, Japan

Received April 23, 2002

A new phosphate, $Ca_9FeD(PO_4)_7$, with a whitlockite-like structure was synthesized by treating $Ca_9Fe(PO_4)_7$ with D_2 at 820 K. Mössbauer spectroscopy showed that the oxidation state of Fe in $Ca_9FeD(PO_4)_7$ is +2. $Ca_9FeD(PO_4)_7$ was paramagnetic in a temperature range from 5 to 300 K with an effective magnetic moment of 4.97 μ_B per Fe^{2+} ion. The infrared spectrum of $Ca_9FeD(PO_4)_7$ exhibited a broad absorption band due to an O−D stretching vibration at 2225 cm^{-1} in addition to bands assigned to PO_4 groups. $Ca_9FeD(PO_4)_7$ was stable under an Ar atmosphere up to 840 K. Above this temperature, it decomposed to a β-$Ca_3(PO_4)_2$-like phase, $Ca_{9.333}Fe_{1.167}(PO_4)_7$, as well as β-$Ca_2P_2O_7$ with releasing D_2O and keeping the oxidation state of +2 for Fe. $Ca_9FeD(PO_4)_7$ liberated D_2O in air above ca. 720 K to produce $Ca_9Fe(PO_4)_7$. Second-harmonic-generation signals, $I_{2\omega}/I_{2\omega}(SiO_2)$, in $Ca_9FeD(PO_4)_7$ (ca. 0.15) were by a factor of ca. 17 less than ca. 2.5 in $Ca_9Fe(PO_4)_7$. Rietveld analysis of time-of-flight neutron diffraction data for $Ca_9FeD(PO_4)_7$ on the basis of space group $R3c$ gave lattice parameters a = 10.369 21(9) Å and c = 37.1289(3) Å, making it possible to locate D atoms at two positions and propose a mechanism of reducing $Ca_9Fe(PO_4)_7$. Its reduction accompanies changes in orientation of parts of $P1O_4$ tetrahedra, formation of O11−D1···O21 and O11′−D2···O34 bonds, and static disordering of Ca^{2+} ions at the Ca3 site. Structure parameters of $Ca_{9.333}Fe_{1.167}(PO_4)_7$ in a product of thermal decomposition of $Ca_9FeD(PO_4)_7$ under Ar were also refined with its X-ray powder diffraction data: space group $R3c$; a = 10.3576(2) Å and c = 37.1429(5) Å; Z = 6. Ca^{2+} and Fe^{2+} ions were found to split into two pieces along the c-axis to occupy a 6a site.

Introduction

Phosphates containing transition metals have been widely investigated because of the variety of their applications and diverse networks including porous ones. These phosphates are used as heterogeneous catalysts[1] and corrosion inhibitors.[2] They are also potential materials for fossil energy conversion,[3] sensing gases,[4] and purification of gas mixtures by removing H_2.[5]

$NaZr_2(PO_4)_3$- (NASICON[6]) and β-$Ca_3(PO_4)_2$-type[7,8] phosphates containing multivalent transition metals undergo redox reactions without destroying fundamental structures owing to high stabilities of their frameworks. Redox systems such as $Cu_{0.5}Zr_2(PO_4)_3$,[9] $Cu_{0.5}Hf_2(PO_4)_3$,[10] $Ca_9Fe(PO_4)_7$,[11−13] $Ca_{9.5}Cu(PO_4)_7$,[14,15] and $Ca_9Na_{1.5}Fe_{0.5}(PO_4)_7$[16] have been reported in the literature. Redox catalysts of the $NaZr_2(PO_4)_3$- and β-$Ca_3(PO_4)_2$-type structures include $CuZr_2(PO_4)_3$,[17] $CuTh_2(PO_4)_3$,[18] $AgZr_2(PO_4)_3$,[19] $AgHf_2(PO_4)_3$,[20] $AgTh_2(PO_4)_3$,[21] $Ca_{3-x}Co_x(PO_4)_2$ ($0 \le x \le 0.31$),[22] $Ca_{3-x}Ni_x(PO_4)_2$ ($0 \le x$

* Corresponding author. Telephone: +81 (298) 51-3354 (ext. 511). Fax: +81 (298) 52-7449. E-mail: IZUMI.Fujio@nims.go.jp.
† National Institute for Materials Science.
‡ Moscow State University.
§ High Energy Accelerator Research Organization.
|| Postdoctoral fellow from Department of Chemistry, Moscow State University, Leninsky Gory, Moscow 119899, Russia.

(1) (a) Millet, J.-M. M. *Catal. Rev.* **1998**, *40*, 1. (b) Bonnet, P.; Millet, J.-M. M.; Leclercq, C.; Vedrine, J. C. *J. Catal.* **1996**, *158*, 128.
(2) (a) Warburton, Y. J.; Gibbon, D. L.; Jackson, K. M.; Gate, L. F.; Rodnyansky, A.; Warburton, P. R. *Corrosion* **1999**, *55*, 898. (b) Bridson, J. N.; Quinlan, S. E.; Tremaine, P. R. *Chem. Mater.* **1998**, *10*, 763. (c) Gorecki, G. *Corrosion* **1992**, *48*, 613.
(3) Safonov, M. S.; Lazoryak, B. I.; Pozharskii, S. B.; Dashkov, S. B. *Dokl. Acad. Nauk. Russ.* **1994**, *358*, 663.
(4) Lazoryak, B. I. In *Fundamental Study of New Materials and Processes in the Substance* (in Russian); Moscow State University Press: Moscow, 1994; p 54.
(5) Lazoryak, B. I.; Morozov, V. A.; Zhdanova, A. N. RF Patent 95100507/26, 1995.
(6) Hagman, L. O.; Kierkegaard, P. *Acta Chem. Scand.* **1968**, *22*, 182.
(7) Dickens, B.; Schroeder, L. W.; Brown, W. E. *J. Solid State Chem.* **1974**, *10*, 232.
(8) Lazoryak, B. I. *Russ. Chem. Rev.* **1996**, *65*, 287.
(9) Le Polles, G.; El Jazouli, A.; Olazcuaga, R.; Dance, J. M.; Le Flem, G.; Hagenmuller, P. *Mater. Res. Bull.* **1987**, *22*, 1171.
(10) Ziyad, M.; Ahmamouch, R.; Rouimi, M.; Gharbage, S.; Vedrine, J. C. *Solid State Ionics* **1998**, *110*, 311.
(11) Lazoryak, B. I.; Morozov, V. A.; Belik, A. A.; Khasanov, S. S.; Shekhtman, V. Sh. *J. Solid State Chem.* **1996**, *122*, 15.
(12) Lazoryak, B. I.; Morozov, V. A.; Safonov, M. S.; Khasanov, S. S. *Mater. Res. Bull.* **1995**, *30*, 1269.
(13) Benarafa, A.; Kacimi, M.; Gharbage, S.; Millet, J.-M. M.; Ziyad, M. *Mater. Res. Bull.* **2000**, *35*, 2047.
(14) Benarafa, A.; Kacimi, M.; Coudurier, G.; Ziyad, M. *Appl. Catal. A* **2000**, *196*, 25.
(15) Lazoryak, B. I.; Khan, N.; Morozov, V. A.; Belik, A. A.; Khasanov, S. S. *J. Solid State Chem.* **1999**, *145*, 345.
(16) Strunenkova, T. V.; Morozov, V. A.; Khasanov, S. S.; Pokholok, K. V.; Zhdanova, A. N.; Lazoryak, B. I. *Crystallogr. Rep.* **1997**, *42*, 64.
(17) Serghini, A.; Brochu, R.; Ziyad, M.; Loukah, M.; Vedrine, J. C. *J. Chem. Soc., Faraday Trans.* **1991**, *87*, 2487.

10.1021/cm020411+ CCC: $22.00
Published on Web 08/01/2002

≤ 0.33),[23,24] $Ca_{10.5-x}Cu_x(PO_4)_7$, and $Ca_{10-x/2}Na_xCu_{0.5}(PO_4)_7$ ($0 \leq x \leq 1$).[14]

Among the phosphates described above, iron phosphates are of considerable importance in view of the high natural abundance of Fe and their hydrogen-absorbing properties. In previous structure refinements of $Ca_9Fe(PO_4)_7$ and $Ca_9FeH_{0.9}(PO_4)_7$,[11] these two were both regarded as being structurally related to β-$Ca_3(PO_4)_2$ (hexagonal, space group $R3c$).[7] However, during the course of an investigation of a redox reaction involving $Ca_9FeH_x(PO_4)_7$ ($0 \leq x \leq 1$), we noticed subtle structural differences between $Ca_9Fe(PO_4)_7$ and $Ca_9FeH_x(PO_4)_7$. Possible locations of H atoms in $Ca_9FeH_{0.9}(PO_4)_7$[11] and related compounds, $Ca_9MH(PO_4)_7$ (M = Mg[25] and Mn[26]), were proposed by analyzing P−O bond lengths and orientations of phosphate ions without any neutron diffraction experiments.

In this work, we have studied the physical and chemical behavior of $Ca_9FeD(PO_4)_7$ prepared by treating $Ca_9Fe(PO_4)_7$ with D_2 at high temperature. We have also refined its structure parameters from time-of-flight (TOF) neutron powder diffraction data to acquire significant information about locations of D atoms and structural changes accompanying the redox reaction in the $Ca_9FeD_x(PO_4)_7$ system. The resulting crystal data have helped us gain a clear understanding of the mechanism of the redox reaction in this system.

Experimental Section

Synthesis. $Ca_9Fe(PO_4)_7$ was prepared from a mixture of $Ca_2P_2O_7$, $CaCO_3$, and Fe_2O_3 by the solid-state method at 1300 K for 150 h with several intermediate grindings. $Ca_9FeD(PO_4)_7$ was synthesized by treating $Ca_9Fe(PO_4)_7$ with D_2. $Ca_9Fe(PO_4)_7$ was placed in a quartz crucible and reduced in a steel setup at 820 K for 48 h. D_2 was added into the setup until the pressure inside the setup remained virtually constant. The maximum D_2 pressure in the setup was 0.2 MPa. $Ca_9FeH(PO_4)_7$ was prepared by reducing $Ca_9Fe(PO_4)_7$ in a flowing H_2 gas at 820 K for 12 h. No impurities could be detected in any significant amount by X-ray powder diffraction (XRD). $Ca_9Fe(PO_4)_7$ was light red, while $Ca_9FeD(PO_4)_7$ and $Ca_9FeH(PO_4)_7$ were white.

Measurements of Physical Properties. We measured ^{57}Fe Mössbauer spectra using a constant-acceleration Mössbauer spectrometer coupled with a multichannel analyzer with a ^{57}Co/Rh source kept at room temperature (RT). All the isomer shifts, δ, were determined with reference to α-Fe. The resulting spectra were decomposed into symmetric quadrupole doublets with Lorentzian profile shapes by least-squares fitting.

Magnetic susceptibilities, χ, of $Ca_9FeD(PO_4)_7$ were measured on a dc SQUID magnetometer (Quantum Design, MPMS) between 5 and 300 K in an applied field of 100 Oe (1 Oe = $[10^3/4\pi]$ A m^{-1}) under both zero-field-cooled (ZFC) and field-cooled (FC) conditions.

IR spectra of samples were recorded on a Nicolet Magna-750 Fourier spectrometer in a wavenumber ($\tilde{\nu}$) range from 4000 to 400 cm^{-1} with the KBr pellet technique.

Second-harmonic-generation (SHG) responses of polycrystalline $Ca_9FeD(PO_4)_7$ were measured in a reflection mode. A Q-switch pulsed Nd:YAG laser operated at a wavelength of λ_ω = 1064 nm was used as a radiation source with a repetition rate of 4 impulses per second and a duration of impulses of about 12 ns. The laser beam was split into two beams to excite the radiation at the halved wavelength, $\lambda_{2\omega}$, of 532 nm simultaneously in the samples to be measured and a reference material, polycrystalline α-SiO_2. The incident-beam peak power was about 0.1 MW on a spot 3 mm in diameter on the surface of the sample. SHG signals, $I_{2\omega}/I_{2\omega}(SiO_2)$, were measured between 300 and 970 K.

Thermogravimetry. Thermal decomposition of $Ca_9FeD(PO_4)_7$ was examined by thermogravimetry (TG) with a Sartorius scale in a quartz reactor in flowing gases, Ar or air, with a gas-flow rate of ca. 10 dm^3/h and a heating rate of ca. 5 K/min. Ar was cleaned by activated carbon kept in liquid N_2.

X-ray and TOF Neutron Powder Diffraction Experiments and Structure Refinements. XRD data of the products were measured at RT on a SIEMENS D500 Bragg−Brentano-type powder diffractometer operated at 30 kV and 30 mA. The diffractometer was equipped with an incident-beam quartz monochromator to obtain Cu $K\alpha_1$ radiation (λ = 1.5406 Å) and a BRAUN position-sensitive detector. Si (NIST Standard Reference Material 640b) was used as an external standard material for diffraction angles. XRD data for phase identification were taken in a 2θ range from 10° to 60° with a step interval of 0.02°. XRD data for structure refinements were collected in a 2θ range from 10° to 110° with a step interval of 0.02°.

Structure parameters were refined from the XRD data by the Rietveld method[27] with RIETAN-2000.[28] Coefficients for an analytical approximation to atomic scattering factors for Ca, Fe, P, and O were taken from ref 29. The split pseudo-Voigt function of Toraya[30] was fit to each reflection profile, and a 11th-order Legendre polynomial was fit to the background. Partial profile relaxation[28] was applied to 012, 104, 110, and 02*10* reflections to improve fits in these reflections at the last stages of the structure refinements. Preferred orientation was corrected with the March−Dollase function on the assumption of a (001) cleavage plane.

TOF neutron powder diffraction data of $Ca_9FeD(PO_4)_7$ were measured at RT on the powder diffractometer Vega[31] ($\Delta d/d \approx 2 \times 10^{-3}$; d is the spacing of lattice plane) at the pulsed spallation neutron facility KENS. About 4.8 g of the sample was contained in a V holder (diameter 9.2 mm), which was slowly rotated during the measurement. An array of 160 position-sensitive detectors (PSDs) installed in a backward bank with a 2θ range from 150° to 170° was used to measure the intensity data. Incident neutron spectra were monitored with a ^{3}He monitor counter. Differences in efficiency between the PSDs and the monitor counter were corrected with intensity data collected in a separate measurement of incoherent scattering from V.

Neutron powder diffraction data in a d range from 0.5 to 5.0 Å were analyzed by the Rietveld method with RIETAN-2001T.[32] A composite background function, i.e., a 14th-order

(18) Arsalane, S.; Kacimi, M.; Ziyad, M.; Coudurier, G.; Vedrine, J. C. *Appl. Catal. A* **1994**, *114*, 243.
(19) Arsalane, S.; Ziyad, M.; Coudurier, G.; Vedrine, J. C. *J. Catal.* **1996**, *159*, 162.
(20) Brik, Y.; Kacimi, M.; Bozon-Verduraz, F.; Ziyad, M. *Microporous Mesoporous Mater.* **2001**, *43*, 103.
(21) Ziyad, M.; Arsalane, S.; Kacimi, M.; Coudurier, G.; Millet, J. M.; Vedrine, J. C. *Appl. Catal. A* **1996**, *147*, 363.
(22) Legrouri, A.; Romdhane, S. S.; Lenzi, J.; Lenzi, M.; Bonel, G. *J. Mater. Sci.* **1996**, *31*, 2469.
(23) (a) Attali, S.; Vigouroux, B.; Lenzi, M.; Perscia, J. *J. Catal.* **1980**, *63*, 496. (b) Legrouri, A.; Lenzi, J.; Lenzi, M. *J. Therm. Anal.* **1993**, *39*, 1321. (c) Lee, S. J.; Jun, J. H.; Lee, S.-H.; Yoon, K. J.; Lim, T. H.; Nam, S.-W.; Hong, S.-A. *Appl. Catal. A* **2002**, *230*, 61.
(24) (a) The Dow Chemical Co.; Vrieland, G. E. US Patent 3, 935, 126, 1974. (b) General Electric Co.; Krabbenhoft, H. O. US Patent 4, 346, 249, 1981. (c) General Electric Co.; Krabbenhoft, H. O. US Patent 4, 366, 089, 1981. (d) The Dow Chemical Co.; Strickler, G. R. US Patent 4, 471, 146, 1983.
(25) Gopal, R.; Calvo, C.; Ito, J.; Sabine, W. K. *Can. J. Chem.* **1974**, *52*, 1155.
(26) Kostiner, E.; Rea, J. R. *Acta Crystallogr., Sect. B* **1976**, *B32*, 250.
(27) Rietveld, H. M. *J. Appl. Crystallogr.* **1969**, *2*, 65.
(28) Izumi, F.; Ikeda, T. *Mater. Sci. Forum* **2000**, *321−324*, 198.
(29) *International Tables for Crystallography*; Kluwer: Dordrecht, 1999; Vol. C, pp 572−574.
(30) Toraya, H. *J. Appl. Crystallogr.* **1990**, *23*, 485.
(31) Kamiyama, T.; Oikawa, K.; Tsuchiya, N.; Osawa, M.; Asano, H.; Watanabe, N.; Furusaka, M.; Satoh, S.; Fujikawa, I.; Ishigaki, T.; Izumi, F. *Physica B* **1995**, *213−214*, 875.
(32) Ohta, T.; Izumi, F.; Oikawa, K.; Kamiyama, T. *Physica B* **1997**, *234−236*, 1093.

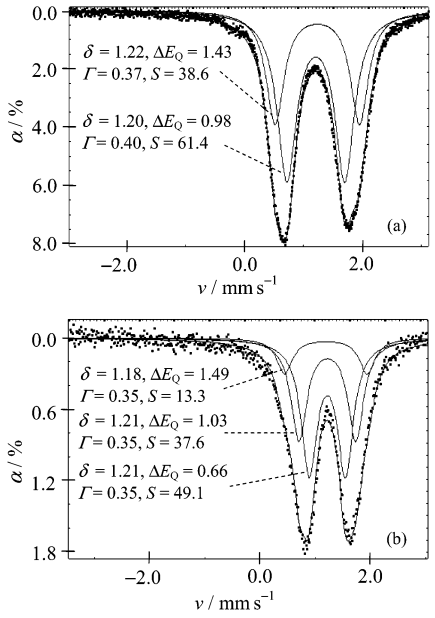

Figure 1. Mössbauer spectra for (a) $Ca_9FeD(PO_4)_7$ and (b) CaFe−Ar at RT. *v*, velocity; α, absorption. Hyperfine parameters refined by least-squares fitting are included in the figure, where δ is the isomer shift, ΔE_Q is the quadrupole splitting, Γ is the full width at half-maximum, and *S* is the area of a profile (%). Unit for δ, ΔE_Q, and Γ: mm/s.

Legendre polynomial multiplied by a smoothed incident spectrum, was fit to the background. Bound coherent scattering lengths, b_c, used for the structure refinements were 4.70 (Ca), 9.45 (Fe), 5.13 (P), 6.671 (D), and 5.803 fm (O).[33] Preferred orientation was corrected with the March−Dollase function on the assumption of a (001) cleavage plane.

Results

Characterization of $Ca_9FeD(PO_4)_7$. Figure 1a presents the Mössbauer spectrum of $Ca_9FeD(PO_4)_7$ comprising two doublets with $\delta \approx 1.20$ mm/s, which provides corroborative evidence that Fe in $Ca_9FeD(PO_4)_7$ has the oxidation state of +2. A similar Mössbauer spectrum was obtained in the case of $Ca_9FeH(PO_4)_7$.

A plot of $(\chi - \chi_0)^{-1}$ against temperature, *T*, for $Ca_9FeD(PO_4)_7$ (Figure 2) obeyed the modified Curie−Weiss rule in the whole temperature range, 5−300 K:

$$(\chi - \chi_0)^{-1} = (T - \theta)/C \qquad (1)$$

where χ_0 is the temperature-independent term including a diamagnetic constituent and Van Fleka paramagnetism, θ is the Weiss constant, and *C* is the Curie constant. $Ca_9FeD(PO_4)_7$ is therefore paramagnetic over the whole range of temperature. The effective magnetic moment, $\mu_e = (8C)^{1/2}$, was calculated at 4.97 μ_B (μ_B, Bohr magneton) per Fe^{2+} ion. This value is close to a theoretical one, 4.90 μ_B, expected for the free Fe^{2+} ion.

As described above, $Ca_9FeD(PO_4)_7$ was the exclusive product of reducing $Ca_9Fe(PO_4)_7$. This finding, coupled with the results of Mössbauer spectroscopy and the magnetic-susceptibility measurements, supports the idea that the oxidation state of Fe changes from +3 to +2 on the reduction of $Ca_9Fe(PO_4)_7$ with D_2 at 870 K:

$$2Ca_9Fe^{3+}(PO_4)_7 + D_2 = 2Ca_9Fe^{2+}D(PO_4)_7 \qquad (2)$$

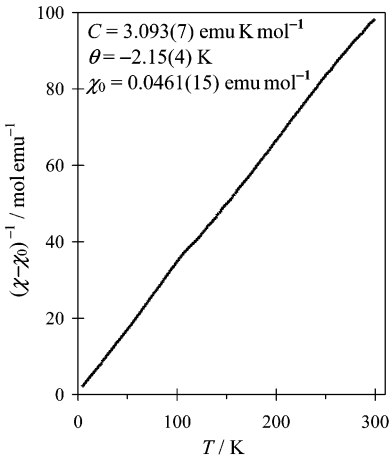

Figure 2. Inverse magnetic susceptibility, $(\chi - \chi_0)^{-1}$, plotted against temperature for $Ca_9FeD(PO_4)_7$ with a zero-field-cooling mode in an applied field of 100 Oe. Parameters in eq 1 are given in the figure.

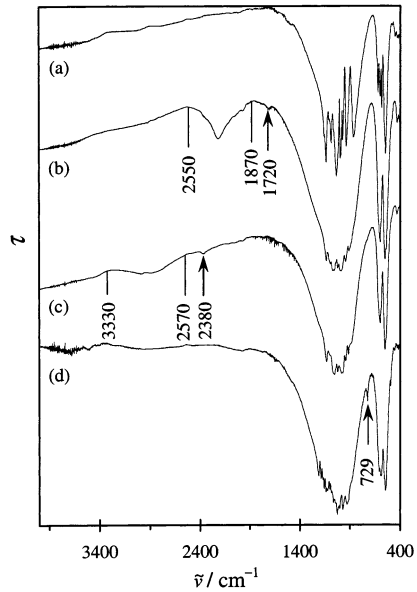

Figure 3. IR spectra in a $\tilde{\nu}$ region from 4000 to 400 cm^{-1} for (a) $Ca_9Fe(PO_4)_7$, (b) $Ca_9FeD(PO_4)_7$, (c) $Ca_9FeH(PO_4)_7$, and (d) CaFe−Ar with τ denoting the transmittance (arbitrary unit). Bands assigned to O−D, O−H, and P−O−P stretching vibrations as well as their regions are marked with arrows and lines, respectively.

When the reduction is complete, the limiting formula of $Ca_9FeD(PO_4)_7$ is reached.

The IR spectrum of $Ca_9FeD(PO_4)_7$ (Figure 3b) showed a broad absorption band due to O−D stretching in a $\tilde{\nu}$ range from 2550 to 1870 cm^{-1} with a maximum at 2225 cm^{-1}, a weak O−D stretching band at 1720 cm^{-1}, and P−O stretching and O−P−O bending bands in a $\tilde{\nu}$ range from 1700 to 450 cm^{-1}. The IR spectrum for $Ca_9FeH(PO_4)_7$ (Figure 3c) exhibited a broad and weak absorption band assigned to an O−H stretching vibration in a $\tilde{\nu}$ range between 3330 and 2570 cm^{-1} and a weak O−H stretching band at 2380 cm^{-1} in addition to P−O stretching and O−P−O bending bands. The wavenumbers of 2550−1870 cm^{-1} and 1720 cm^{-1} in $Ca_9FeD(PO_4)_7$

(33) Sears, V. F. *International Tables for Crystallography*, 2nd ed.; Kluwer: Dordrecht, 1999; Vol. C, pp 440−450.

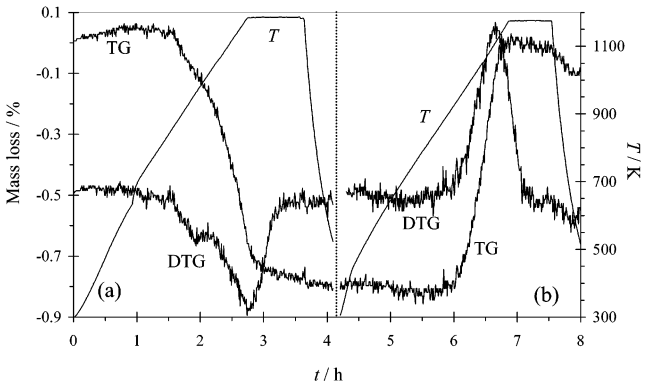

Figure 4. *T*, TG, and DTG versus time (*t*) curves (a) for $Ca_9FeD(PO_4)_7$ under Ar and (b) for CaFe−Ar under air (see reactions 4 and 5).

and those of 3330−2570 cm^{-1} and 2380 cm^{-1} in $Ca_9FeH(PO_4)_7$ were consistent with the $\tilde{\nu}$ ratio expected for deuteroxyl and hydroxyl groups in the simple harmonic approximation: $\tilde{\nu}(O-H)/\tilde{\nu}(O-D) = 1.37$.[34] Hence, the bands at 1720 and 2380 cm^{-1} are assigned to O−D and O−H stretching vibrations, respectively. O−H stretching bands for HPO_4^{2-} appear between 3400 and 2000 cm^{-1}.[35] In perovskite-type oxides $Sr(Ce_xZr_{1-x})_{0.95}Yb_{0.05}O_3$, O−H stretching bands occur between 3350 and 2350 cm^{-1}.[36]

The IR spectra for $Ca_9FeD(PO_4)_7$ and $Ca_9FeH(PO_4)_7$ were very similar to each other in the $\tilde{\nu}$ range of the P−O stretching and O−P−O bending bands (Figure 3b,c). On the other hand, they differed considerably from the IR spectrum of $Ca_9Fe(PO_4)_7$ (Figure 3a), which resembled that of $Sr_9Fe(PO_4)_7$.[37]

Redox Reactions and Thermal Decomposition Involving $Ca_9FeD(PO_4)_7$. Heating $Ca_9FeD(PO_4)_7$ in air up to 1200 K is believed to change the oxidation state of Fe from +2 to +3. The light-red product was $Ca_9Fe(PO_4)_7$, whose IR spectrum did not show any bands due to the O−D stretching vibration. $Ca_9FeD(PO_4)_7$ therefore reacts with O_2 to yield $Ca_9Fe(PO_4)_7$, thereby releasing D_2O:

$$4Ca_9FeD(PO_4)_7 + O_2 = 4Ca_9Fe(PO_4)_7 + 2D_2O \quad (3)$$

Figure 4a gives TG and differential TG (DTG) curves for $Ca_9FeD(PO_4)_7$ in an Ar atmosphere. $Ca_9FeD(PO_4)_7$ was stable under Ar up to 840 K. Above this temperature, we observed about 0.84% loss in mass, which is practically the same as ca. 0.83% evaluated on the assumption of a thermal decomposition formulated

$$14Ca_9FeD(PO_4)_7 = 12Ca_{9.333}Fe_{1.167}(PO_4)_7 + 7Ca_2P_2O_7 + 7D_2O \quad (4)$$

In what follows, the product resulting from heating $Ca_9FeD(PO_4)_7$ in Ar will be referred to as CaFe−Ar.

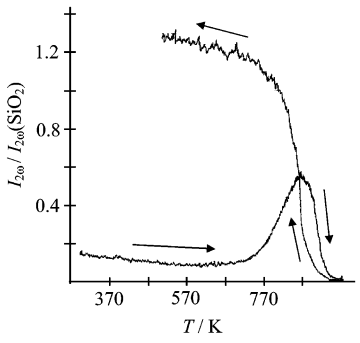

Figure 5. Dependence of the SHG signals, $I_{2\omega}/I_{2\omega}(SiO_2)$, on temperature for $Ca_9FeD(PO_4)_7$ in air. Arrows indicate heating and cooling curves.

The Mössbauer spectrum of CaFe−Ar (Figure 1b) obviously demonstrated that Fe has the oxidation state of +2. CaFe−Ar was white with a pale-green tint. Accordingly, the oxidation state of Fe remained unaltered during reaction 4. XRD showed CaFe−Ar to contain a β-$Ca_3(PO_4)_2$-like phase as well as β-$Ca_2P_2O_7$ in conformity with reaction 4. The mass fraction of β-$Ca_2P_2O_7$ was determined in two ways: (a) from scale factors refined in the Rietveld refinements (see below) and (b) by an internal standard method. In method b, we used the 012 and 113 reflections of corundum (Al_2O_3) and the strongest 008 reflection of β-$Ca_2P_2O_7$. Methods a and b afforded mass fractions of ca. 7.7% and ca. 11.3%, respectively. The latter value was comparable to the mass fraction of ca. 11.8% calculated with reaction 4. In the IR spectrum of CaFe−Ar (Figure 3d), a band due to a P−O−P stretching vibration in β-$Ca_2P_2O_7$[35] appeared at 729 cm^{-1}, but no noticeable O−D stretching band was observed.

All the above facts concerning CaFe−Ar justify the validity of reaction 4, and the measured loss in mass agreed well with the stoichiometric composition $Ca_9FeD(PO_4)_7$. $Ca_9MgH(PO_4)_7$ was thermally more stable than $Ca_9FeD(PO_4)_7$. $Ca_9MgH(PO_4)_7$ decomposed in an N_2 atmosphere in a *T* range from 920 to 1400 K.[25]

Figure 4b illustrates TG and DTG curves in air for CaFe−Ar. An increase in mass of ca. 0.79% is close to the value of ca. 0.75% calculated with the probable reaction

$$24Ca_{9.333}Fe_{1.167}(PO_4)_7 + 14Ca_2P_2O_7 + 7O_2 = 28Ca_9Fe(PO_4)_7 \quad (5)$$

The oxidation of CaFe−Ar gave rise to a β-$Ca_3(PO_4)_2$-like phase, $Ca_9Fe(PO_4)_7$. When CaFe−Ar was heated at 1300 K under Ar for 40 h and then oxidized in air, Fe_2O_3 was formed as an impurity. Nevertheless, further annealing at 1300 K caused complete disappearance of Fe_2O_3 and regeneration of $Ca_9Fe(PO_4)_7$.

Figure 5 is a plot of the SHG signals, $I_{2\omega}/I_{2\omega}(SiO_2)$, against temperature for $Ca_9FeD(PO_4)_7$. The increase in the SHG signal above ca. 720 K is presumably caused by the onset of oxidizing $Ca_9FeD(PO_4)_7$. The decrease in the SHG signal above ca. 870 K and its final disappearance are associated with a polar-to-centrosymmetric phase transition in $Ca_9Fe(PO_4)_7$.[38] During the cooling of oxidized $Ca_9Fe(PO_4)_7$, the SHG signal increased with decreasing temperature. SHG signals of ca. 0.15 in $Ca_9FeD(PO_4)_7$ were by a factor of ca. 17 less

(34) Nakamoto, K. *Infrared Spectra of Inorganic and Coordination Compounds*; Wiley: New York, 1963.
(35) Nyquist, R. A.; Kagel, R. O. *Infrared Spectra of Inorganic Compounds*; Academic Press: New York, 1971.
(36) Sata, N.; Yugami, H.; Akiyama, Y.; Sone, H.; Kitamura, N.; Hattori, T.; Ishigame, M. *Solid State Ionics* **1999**, *125*, 285.
(37) Belik, A. A.; Izumi, F.; Ikeda, T.; Okui, M.; Malakho, A. P.; Morozov, V. A.; Lazoryak, B. I. Accepted for publication in *J. Solid State Chem.*

than ca. 2.5 in $Ca_9Fe(PO_4)_7$.[38] Such pronounced differences in SHG signals must arise from structural differences between $Ca_9FeD(PO_4)_7$ and $Ca_9Fe(PO_4)_7$. Though the SHG signals in $Ca_9FeD(PO_4)_7$ were weak, they unambiguously reveal $Ca_9FeD(PO_4)_7$ to be noncentrosymmetric.

Structure Refinement of $Ca_9FeD(PO_4)_7$. Indexing Bragg reflections in the X-ray and neutron powder diffraction patterns of $Ca_9FeD(PO_4)_7$ showed it to crystallize in the trigonal system with lattice parameters of $a \approx 10.35$ Å and $c \approx 37.17$ Å. Reflection conditions derived from the indexed reflections were $-h + k + l = 3n$ for hkl and $h + l = 3n$, $l = 2n$ for $h\bar{h}l$ (obverse setting), affording possible space groups $R3c$ (No. 161, noncentrosymmetric) and $R\bar{3}c$ (No. 167, centrosymmetric). As described above, the SHG data exclude the possibility for $Ca_9FeD(PO_4)_7$ to have space group $R\bar{3}c$.

For initial fractional coordinates in Rietveld analysis of $Ca_9FeD(PO_4)_7$, we used those of $Ca_9FeH_{0.9}(PO_4)_7$, which was regarded as possessing a β-$Ca_3(PO_4)_2$-like structure with space group $R3c$ and lattice parameters of $a = 10.3543(2)$ Å and $c = 37.168(1)$ Å.[11] The Fe5 site (6*a*; 0, 0, *z*) was placed at the origin ($z = 0$) owing to the arbitrariness of setting the origin in the noncentrosymmetric space group of $R3c$. We assigned isotropic atomic displacement parameters, *U*, to all the sites, with *U* included in the isotropic Debye−Waller factor in the form of $\exp(-2\pi^2 U/d^2)$. Some *U* parameters converged to unusually large or negative values. In addition, some P−O bond lengths, l(P−O), in particular l(P1−O11) ≈ 2.1 Å, were much larger or shorter than would be expected for a P−O bond. These findings suggest that the above structural model has to be modified to some extent.

Next, we used fractional coordinates of synthetic whitlockite, $Ca_9MgH(PO_4)_7$,[25] in the initial structural model, which differed from the β-$Ca_3(PO_4)_2$ model in orientation of $P1O_4$ tetrahedra about the 3-fold rotation axis, namely, the *c*-axis. D atoms were located at a general position (18*b*; $x \approx 0.06$, $y \approx 0.10$, and $z \approx 0.192$) near a line connecting O11 (6*a*; $z \approx 0.203$) and O21 (18*b*; $x \approx 0.724$, $y \approx 0.905$, and $z \approx 0.176$) with an occupancy, *g*, of 1/3, as suggested in $Ca_9MgH(PO_4)_7$.[25] The Rietveld refinement adopting the whitlockite model gave more reasonable *U* and l(P−O) values. However, an l(P1−O11) value of 1.69 Å and *U* parameters of P1 at a 6*a* site (3.56 nm^2), O11 (3.20 nm^2), Ca3 at a 18*b* site (2.06 nm^2), and D (8.2 nm^2) were still too large. Refining the occupancy, *g*, and *U* for D atoms yielded g(D) = 0.284(8) and U(D) = 5.2(6) nm^2. The refinement of anisotropic atomic displacement parameters, U_{11} and U_{33}, for P1 at this stage led to $U_{33} \approx 50U_{11}$. Such thermal motion that appears to be extremely anisotropic must reflect disordering of the P1 atoms along the *c*-axis.

We modified the above structural model by trial and error and found two configurations of Ca3 atoms and $P1O_4$ tetrahedra. One atomic configuration is similar to that in whitlockite, viz., Ca3 (18*b*; $x \approx 0.142$, $y \approx 0.309$, and $z \approx 0.330$), P1 (6*a*; $z \approx 0.246$), O11 (6*a*; $z \approx 0.204$), and O12 (18*b*; $x \approx 0.022$, $y \approx 0.871$, and $z \approx 0.259$). The other atomic configuration resembles that in β-$Ca_3(PO_4)_2$, i.e., Ca3′ (18*b*; $x \approx 0.127$, $y \approx 0.271$, and $z \approx 0.326$), P1′ (6*a*; $z \approx 0.268$), O11′ (6*a*; $z \approx 0.311$), and O12′ (18*b*; $x \approx 0.001$, $y \approx 0.861$, and $z \approx 0.251$). We refined occupancies and *U* parameters for the Ca3 and Ca3′ sites under linear constraints of g(Ca3) + g(Ca3′) = 1 and U(Ca3) = U(Ca3′). The following linear constraints were imposed on occupancies and *U* parameters of atoms belonging the $P1O_4$ and $P1'O_4$ tetrahedra: g(P1) = g(O11) = g(O12) = 1 − g(P1′) = 1 − g(O11′) = 1 − g(O12′), U(P1) = U(P1′), and U(O12) = U(O12′).

In the preliminary refinement, D atoms proved to lie aside two lines connecting O11 with O21 (D1: 18*b*; $x \approx 0.06$, $y \approx 0.10$, and $z \approx 0.193$) and O11′ with O34 (D2: 18*b*; $x \approx 0.10$, $y \approx 0.06$, and $z \approx 0.315$). Then, linear constraints, g(D1) = g(O11)/3, g(D2) = g(O11′)/3, and U(D1) = U(D2), were applied with the assumption of the presence of DPO_4^{2-} ions. Refined lattice and structure parameters yielded bond lengths of l(O11′−D2) ≈ 1.21 Å and l(O34−D2) ≈ 1.26 Å, which are quite unusual for O11′−D2···O34 bonds with the centered dots expressing a hydrogen bond. A g(D2) value of about 0.07 seemed to be too low to get accurate fractional coordinates of D2. A restraint l(O11′−D2) < 1.0 Å was therefore imposed in the final structure refinement.

Table 1 lists experimental and refinement conditions for the TOF neutron diffraction data, lattice parameters, *R* factors, and so forth. Final fractional coordinates and *U* parameters for $Ca_9FeD(PO_4)_7$ are tabulated in Table 2, and selected interatomic distances calculated with ORFFE[39] are listed in Table 3. Numbers in parentheses are estimated standard deviations of the last significant digits throughout this paper. Figure 6 displays observed, calculated, and difference TOF neutron diffraction patterns for $Ca_9FeD(PO_4)_7$.

Table 1. Conditions of the TOF Neutron Diffraction Experiments and Parts of Refinement Results for $Ca_9FeD(PO_4)_7$

d range/Å	0.5−5.0
no. of data points	3970
space group	*R*3*c* (No. 161)
Z	6
lattice parameters	
a/Å	10.36921(9)
c/Å	37.1289(3)
V/Å^3	3457.27(5)
no. of Bragg reflections	3227
preferred-orientation parameter	1.0424(11)
variables	
structure/lattice	79/2
background/profile	15/12
R_{wp}; R_p	2.50%; 1.97%
R_B; R_F	0.73%; 0.70%
S[a]	1.51

[a] $S = R_{wp}/R_e$.

Structure Refinement of $Ca_{9.333}Fe_{1.167}(PO_4)_7$. We also refined structure parameters of the β-$Ca_3(PO_4)_2$-like phase in CaFe−Ar from its XRD data by the Rietveld method. For the second phase, β-$Ca_2P_2O_7$,[40] only a scale factor and lattice parameters *a* and *c* were refined. Profile parameters of β-$Ca_2P_2O_7$ were constrained to be equal to those of $Ca_{9.333}Fe_{1.167}(PO_4)_7$ (see reaction 4). Fractional coordinates of β-$Ca_3(PO_4)_2$[7] were

(38) Lazoryak, B. I.; Morozov, V. A.; Belik, A. A.; Stefanovich, S. Yu.; Grebenev, V. V.; Leonidov, I. A.; Mitberg, E. B.; Davydov, S. A.; Lebedev, O. I.; Van Tendeloo, G. Submitted for publication in *Chem. Mater*.

(39) Busing, W. R.; Martin, K. O.; Levy H. A. *Report ORNL-TM-306*; Oak Ridge National Laboratory: Oak Ridge, TN, 1964.

(40) Webb, N. C. *Acta Crystallogr.* **1966**, *21*, 942.

Table 2. Fractional Coordinates and Isotropic Atomic Displacement Parameters for $Ca_9FeD(PO_4)_7$

atom	site	*g*	*x*	*y*	*z*	*U*/nm²
Ca1	18*b*	1	0.7215(4)	0.8541(5)	0.4347(2)	0.44(8)
Ca2	18*b*	1	0.6137(4)	0.8207(5)	0.2322(2)	0.73(9)
Ca3	18*b*	0.51(4)	0.1419(13)	0.309(2)	0.3299(4)	0.89(10)[a]
Ca3′	18*b*	0.49[e]	0.1270(13)	0.271(2)	0.3262(3)	0.89[a]
Fe5	6*a*	1	0	0	0	0.43(5)
P1	6*a*	0.778(7)	0	0	0.2462(2)	0.84(14)[b]
P1′	6*a*	0.222[f]	0	0	0.2681(8)	0.84[b]
P2	18*b*	1	0.6838(4)	0.8554(4)	0.1357(2)	0.90(9)
P3	18*b*	1	0.6492(4)	0.8434(4)	0.0325(2)	0.44(8)
O11	6*a*	0.778[g]	0	0	0.2037(3)	2.1(2)
O11′	6*a*	0.222[f]	0	0	0.3106(6)	0.5(5)
O12	18*b*	0.778[g]	0.0224(4)	0.8712(7)	0.2587(2)	0.73(8)[c]
O12′	18*b*	0.222[f]	0.001(3)	0.861(2)	0.2506(6)	0.73[c]
O21	18*b*	1	0.7250(4)	0.9064(3)	0.1749(2)	1.51(8)
O22	18*b*	1	0.7529(4)	0.7672(3)	0.1219(2)	1.02(8)
O23	18*b*	1	0.7287(3)	−0.0008(3)	0.1134(2)	0.74(7)
O24	18*b*	1	0.5121(4)	0.7588(4)	0.13073(14)	0.96(8)
O31	18*b*	1	0.6010(3)	0.9529(3)	0.0461(2)	0.85(7)
O32	18*b*	1	0.5812(4)	0.6936(4)	0.0528(2)	1.19(8)
O33	18*b*	1	0.8212(4)	0.9211(3)	0.03734(14)	0.82(7)
O34	18*b*	1	0.6015(3)	0.8065(4)	0.99290(14)	1.24(7)
D1	18*b*	0.259[h]	0.0619(14)	0.1028(13)	0.1926(6)	5.8(3)[d]
D2	18*b*	0.074[i]	0.103(3)	0.06(3)	0.315(2)	5.8[d]

[a–d] These *U* parameters were constrained to be equal to each other. [e] g(Ca3′) = 1 − g(Ca3). [f] g(P1′) = g(O11′) = g(O12′) = 1 − g(P1). [g] g(O11) = g(O12) = g(P1). [h] g(D1) = g(O11′)/3. [i] g(D2) = g(O11′)/3.

Table 3. Selected Interatomic Distances (Å) in $Ca_9FeD(PO_4)_7$

Ca1−O32	2.314(5)	Ca3−O31	2.335(11)
Ca1−O34	2.415(5)	Ca3−O23	2.380(12)
Ca1−O24	2.438(5)	Ca3−O22	2.413(12)
Ca1−O24a	2.465(5)	Ca3−O21	2.42(2)
Ca1−O31	2.463(6)	Ca3−O34	2.568(14)
Ca1−O23	2.531(5)	Ca3−O32	2.581(13)
Ca1−O22	2.760(5)	Ca3−O34a	2.67(2)
Ca1−O12	2.497(7)	Ca3−O11′	2.87(2)
Ca1−O12′	2.42(2)	Ca3−O12	3.08(2)
Ca2−O21	2.371(5)	Ca3′−O34	2.398(12)
Ca2−O23	2.362(5)	Ca3′−O34a	2.451(14)
Ca2−O33	2.432(6)	Ca3′−O11′	2.51(2)
Ca2−O33a	2.461(5)	Ca3′−O31	2.415(11)
Ca2−O22	2.455(6)	Ca3′−O23	2.435(11)
Ca2−O31	2.640(6)	Ca3′−O22	2.484(11)
Ca2−O32	2.663(6)	Ca3′−O32	2.635(11)
Ca2−O12	2.365(6)	Ca3′−O21	2.71(2)
Ca2−O12′	2.38(2)	Ca3′−O12	2.80(2)
Fe5−O24 (×3)	2.088(4)	Ca3′−O12′	3.15(3)
Fe5−O33 (×3)	2.124(4)	P1′−O11′	1.58(4)
P1−O11	1.577(12)	P1′−O12′ (×3)	1.59(2)
P1−O12 (×3)	1.537(7)	P2−O21	1.535(5)
D1−O11	1.018(13)	P2−O22	1.507(4)
D1−O21	1.715(13)	P2−O23	1.559(5)
O11−O21	2.729(4)	P2−O24	1.556(4)
D2−O11′	0.94(3)	P3−O31	1.536(4)
D2−O34	1.54(3)	P3−O32	1.544(5)
O11′−O34	2.478(6)	P3−O33	1.558(4)
		P3−O34	1.537(5)

used as an initial model in the structure refinement of $Ca_{9.333}Fe_{1.167}(PO_4)_7$. We fixed occupancies of metal sites in $Ca_{9.333}Fe_{1.167}(PO_4)_7$ to impose "chemical" constraints on them: g(Ca1) = 1 (18*b*; $x \approx 0.725$, $y \approx 0.858$, and $z \approx 0.433$), g(Ca2) = 1 (18*b*; $x \approx 0.616$, $y \approx 0.823$, and $z \approx 0.232$), g(Ca3) = 1 (18*b*; $x \approx 0.124$, $y \approx 0.272$, and $z \approx 0.326$), g(Ca) = 1/3 and g(Fe) = 1/6 for a mixed-metal site M4 (6*a*; $z \approx 0.178$), and g(Fe5) = 1 (6*a*; $z = 0$). A Rietveld refinement adopting this model afforded reasonable *U* parameters for all the atoms except for U(Ca1) = −0.08(9) nm² and U(M4) = 14.3(9) nm². The unusually large U(M4) parameter indicates that Ca and Fe atoms at the M4 site split in different degrees along the *c*-axis. Hence, we assigned independent sites to these Ca and Fe atoms, i.e., Ca4 (6*a*; $z \approx 0.19$) with g(Ca4) = 1/3 and Fe4 (6*a*; $z \approx 0.15$) with g(Fe4) = 1/6. More reasonable *U* parameters resulted from the subsequent Rietveld refinement: U(Ca1) = 0.42(10) nm², U(Ca4) = 1.8(5) nm², and U(Fe4) = 3.7(9) nm².

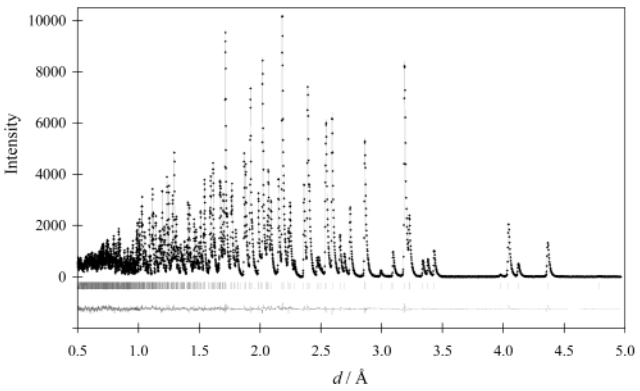

Figure 6. Observed (crosses), calculated (solid line), and difference patterns resulting from the Rietveld analysis of the TOF neutron powder diffraction data for $Ca_9FeD(PO_4)_7$. Bragg reflections are indicated by tick marks. Background intensities were subtracted from the observed and calculated TOF neutron diffraction patterns.

Table 4. Conditions of the XRD Experiments and Parts of Refinement Results for CaFe−Ar

space group	*R*3*c* (No. 161)[a]
Z	6[a]
2θ range/deg	10−110
step width/deg	0.02
I_{max}/counts	53 701
lattice parameters	
a/Å	10.3576(2)[a]
c/Å	37.1429(5)[a]
V/Å³	3450.83(10)[a]
no. of Bragg reflections	488;[a] 695[b]
preferred-orientation parameter	0.8556(14)[a]
variables	
structure/lattice	56/2[a]
background/profile	12/10
PPP[c]	20[a]
R_{wp}; R_p	2.75%; 2.12%
R_B	1.76%;[a] 2.31%[b]
R_F	1.13%;[a] 1.16%[b]
S	1.52

[a] For $Ca_{9.333}Fe_{1.167}(PO_4)_7$. [b] For β-$Ca_2P_2O_7$. [c] Refined primary profile parameters.[28]

Table 4 lists experimental and refinement conditions, lattice parameters, *R* factors, and so forth. Final fractional coordinates and *U* parameters for $Ca_{9.333}Fe_{1.167}(PO_4)_7$ are tabulated in Table 5. Figure 7 displays observed, calculated, and difference XRD patterns for the sample CaFe−Ar.

Discussion

Using the different techniques of characterization, we confirmed the stoichiometric composition of $Ca_9FeD(PO_4)_7$ and the validity of reactions 4 and 5. Mössbauer spectroscopy and magnetic susceptibilities proved the oxidation state of +2 for Fe atoms in $Ca_9FeD(PO_4)_7$. For the final confirmation of the formal Fe valence, we calculated bond valence sums, *V*, of the octahedral Fe5 sites in $Ca_9FeD(PO_4)_7$ and $Ca_{9.333}Fe_{1.167}(PO_4)_7$ from the six Fe5−O bond lengths using two bond valence param-

Table 5. Fractional Coordinates and Isotropic Atomic Displacement Parameters for $Ca_{9.333}Fe_{1.167}(PO_4)_7$

atom	site	*g*	*x*	*y*	*z*	U/nm^2
Ca1	18*b*	1	0.7250(4)	0.8584(5)	0.43288(14)	0.42(10)
Ca2	18*b*	1	0.6161(4)	0.8225(6)	0.23197(14)	0.43(11)
Ca3	18*b*	1	0.1242(5)	0.2719(3)	0.32644(14)	1.62(10)
Ca4	6*a*	1/3	0	0	0.1905(6)	1.8(5)
Fe4	6*a*	1/6	0	0	0.1575(7)	3.7(9)
Fe5	6*a*	1	0	0	0	0.78(11)
P1	6*a*	1	0	0	0.2645(2)	2.0(2)
P2	18*b*	1	0.6838(4)	0.8576(6)	0.1357(2)	0.38(14)
P3	18*b*	1	0.6513(6)	0.8471(7)	0.0324(2)	1.1(2)
O11	6*a*	1	0	0	0.3111(5)	0.23(7)[a]
O12	18*b*	1	0.0097(12)	0.8647(8)	0.2565(3)	0.23[a]
O21	18*b*	1	0.7391(10)	0.9234(9)	0.1732(3)	0.23[a]
O22	18*b*	1	0.7577(14)	0.7740(14)	0.1225(3)	0.23[a]
O23	18*b*	1	0.7250(13)	0.0020(11)	0.1134(2)	0.23[a]
O24	18*b*	1	0.5156(12)	0.7611(14)	0.1330(3)	0.23[a]
O31	18*b*	1	0.6043(12)	0.9535(12)	0.0456(3)	0.23[a]
O32	18*b*	1	0.5738(13)	0.6940(12)	0.0542(3)	0.23[a]
O33	18*b*	1	0.8228(12)	0.9207(14)	0.0413(3)	0.23[a]
O34	18*b*	1	0.6190(9)	0.8196(12)	0.9923(2)	0.23[a]

[a] These U parameters were constrained to be equal to each other.

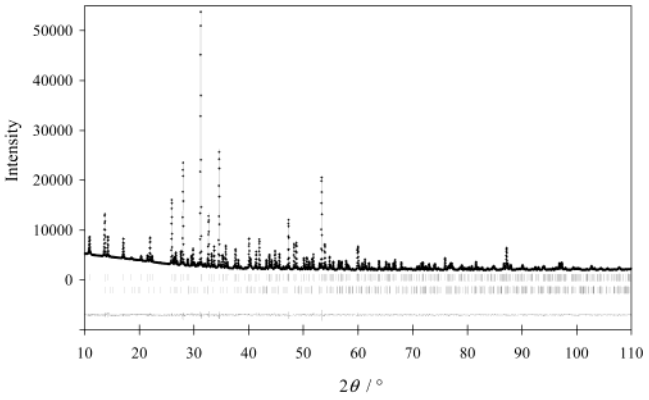

Figure 7. Observed (crosses), calculated (solid line), and difference XRD patterns for CaFe−Ar. Bragg reflections for $Ca_{9.333}Fe_{1.167}(PO_4)_7$ (upper) and β-$Ca_2P_2O_7$ (lower) are indicated by tick marks.

eters, R_0.[41,42] The resulting V values in $Ca_9FeD(PO_4)_7$ and $Ca_{9.333}Fe_{1.167}(PO_4)_7$ were, respectively, 2.20 and 2.08 with $R_0 = 1.734$[41] and 2.08 and 1.96 with $R_0 = 1.713$.[42] These V values offer additional evidence for the oxidation state of +2 for Fe.

We could determine the locations of D atoms, D1 and D2, from the TOF neutron diffraction data thanks to the relatively large b_c value of D. Both D1 and D2 are not isolated but are involved in DPO_4^{2-} ions. The present phosphate is, therefore, best represented as $Ca_9Fe(PO_4)_6(DPO_4)$, where the ratio of the amount of substance of D1 to that of D2 is 0.778:0.222.

Thermal dehydration of $Ca_9MgH(PO_4)_7$ in an N_2 atmosphere proceeds via two main dehydration processes.[25] This experimental fact suggests the occupation of two or more sites by H atoms in $Ca_9MgH(PO_4)_7$. The DTG curve for $Ca_9FeD(PO_4)_7$ (Figure 4a) is also in accord with two processes of releasing D atoms. Figure 8 presents IR spectra of $Ca_9FeD(PO_4)_7$ and $Ca_9FeH(PO_4)_7$ in a $\tilde{\nu}$ range from 4000 to 1600 cm^{-1}. $Ca_9FeH(PO_4)_7$ exhibits at least three O−H stretching bands denoted

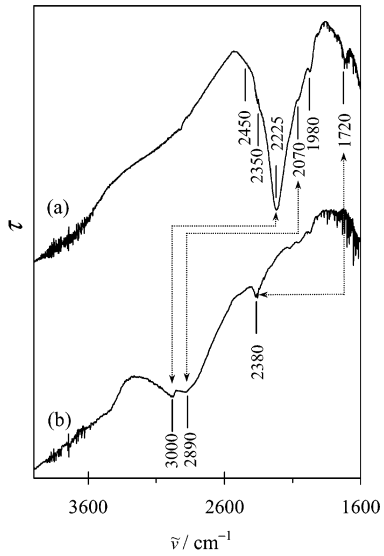

Figure 8. IR spectra of (a) $Ca_9FeD(PO_4)_7$ and (b) $Ca_9FeH(PO_4)_7$ in a $\tilde{\nu}$ region from 4000 to 1600 cm^{-1} with τ denoting the transmittance (arbitrary unit). Tick marks denote absorption bands due to O−H and O−D stretching. Arrows indicate two bands related by the ratio $\tilde{\nu}$(O−H)/$\tilde{\nu}$(O−D) ≈ 1.37.

by tick marks, whereas $Ca_9FeD(PO_4)_7$ shows at least six O−D stretching bands. Pairs of absorption bands with the $\tilde{\nu}$(O−H)/$\tilde{\nu}$(O−D) ratio of 1.37 are indicated by arrows in Figure 8. In perovskite-type oxides $Ba(Zr_{0.9}Y_{0.1})O_3$, $(La_{0.8}Sr_{0.2})ScO_3$, and $Sr(Ce_{0.95}Y_{0.05})O_3$, several O−H (O−D) stretching bands are correlated with different locations of O−H (O−D) groups.[43] Thus, our TG, IR, and crystal data of $Ca_9FeD(PO_4)_7$ are all consistent with the presence of two D sites in $Ca_9FeD(PO_4)_7$.

The crystal data of $Ca_9FeD(PO_4)_7$ afforded quite natural O−D···O bond lengths (Table 3) and bond angles, ϕ(O11−D1−O21) = 174.4(14)° and ϕ(O11′−D2−O34) = 170(4)°.[44] On the use of identical O−O lengths (in O−H···O bonds) in $Ca_9FeH(PO_4)_7$ and an empirical relation between $\tilde{\nu}$(O−H) and l(O−O),[45] the band at 2380 cm^{-1} in the IR spectrum of $Ca_9FeH(PO_4)_7$ (Figure 8) can be assigned to the O11′−H2···O34 bond and the bands at 3000 and 2890 cm^{-1} to the O11−H1···O21 bond.

We fit the Lorentzian doublets to the Mössbauer spectrum of $Ca_9FeD(PO_4)_7$ with comparable initial parameters (Figure 1). At least two distinct Fe positions were found despite the inclusion of only one Fe5 site in the asymmetric unit. This contradiction is explained in terms of the two D sites, orientational disordering of the $P1O_4$ tetrahedra, and Ca^{2+} ions occupying the two positions Ca3 and Ca3′. For example, some O21 atoms form O11−D1···O21 bonds whereas the other O21 atoms do not. The configuration of the O21 atoms influences that of the O24 atoms forming the first coordination sphere of Fe5 (Figure 9).

(41) Brese, R. E.; O'Keeffe, M. *Acta Crystallogr., Sect. B* **1991**, *B47*, 192.
(42) Kanowitz, S. M.; Palenik, G. J. *Inorg. Chem.* **1998**, *37*, 2086.
(43) Glerup, M.; Poulsen, F. W.; Berg, R. W. *Solid State Ionics* **2002**, *148*, 83.
(44) See, for example: (a) Fujihara, T.; Ichikawa, M.; Gustafsson, T.; Olovsson, I.; Tsuchida, T. *J. Phys. Chem. Solids* **2002**, *63*, 309. (b) Hriljac, J. A.; Torardi, C. C.; Vogt, T. *J. Phys. Chem. Solids* **1995**, *56*, 1339. (c) Partin, D. E.; O'Keeffe, M. *J. Solid State Chem.* **1995**, *119*, 157.
(45) Nakamoto, K.; Margoshes, M.; Rundle, R. E. *J. Am. Chem. Soc.* **1955**, *77*, 6480.

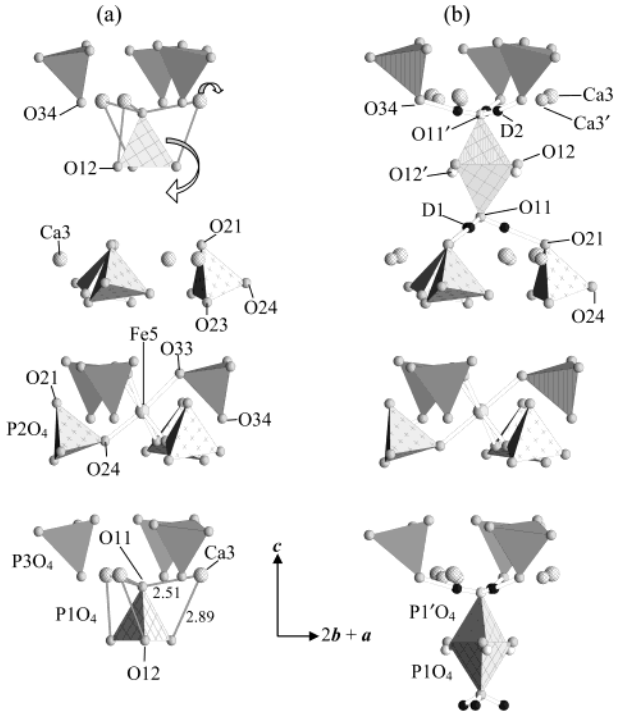

Figure 9. Parts of structures of (a) $Ca_9Fe(PO_4)_7$ and (b) $Ca_9FeD(PO_4)_7$ depicting their differences. Arrows represent movements of constituents during the reduction. Bond lengths are given in angstroms.

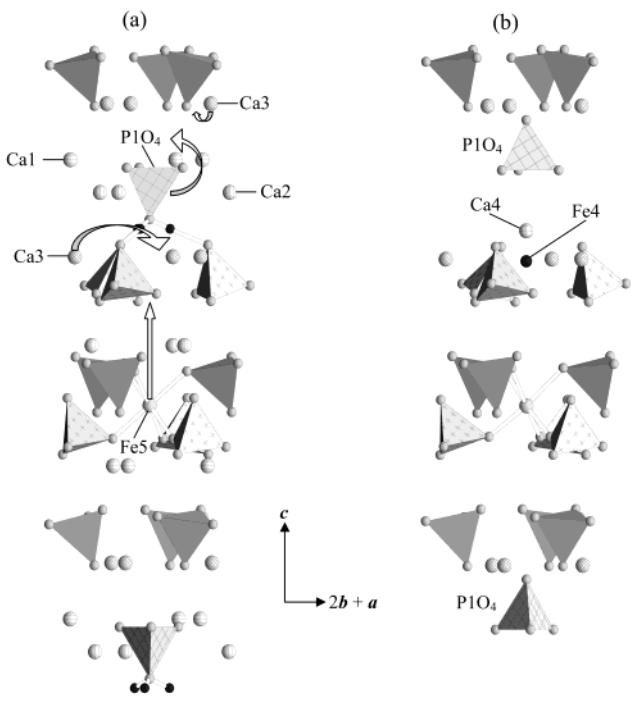

Figure 10. Portions of structures for (a) $Ca_9FeD(PO_4)_7$ and (b) $Ca_{9.333}Fe_{1.167}(PO_4)_7$. Configurations of Ca3 and $P1O_4$ are illustrated for $Ca_9FeD(PO_4)_7$. Arrows represent paths of migration of Ca^{2+} and Fe^{2+} ions to the M4 site and rearrangements of $P1O_4$ tetrahedra and Ca3 atoms during thermal decomposition of $Ca_9FeD(PO_4)_7$ under Ar.

Figure 9 illustrates portions of the structures for $Ca_9Fe(PO_4)_7$[11] and $Ca_9FeD(PO_4)_7$, manifesting their differences unequivocally. In $Ca_9Fe(PO_4)_7$, the O11 and O12 atoms belonging to the $P1O_4$ tetrahedron are bonded to three Ca3 atoms. During the reduction of $Ca_9Fe(PO_4)_7$, $P1O_4$ tetrahedra bearing D atoms change their orientation to form O11−D1···O21 bonds. Because Ca3 atoms are not bonded to O11 in this case, their positions change only slightly. The Ca3 atoms and $P1O_4$ tetahedra are bound to neighboring ions rather loosely in $Ca_9Fe(PO_4)_7$. In fact, the polar-to-centrosymmetric phase transition at 890 K in $Ca_9Fe(PO_4)_7$ accompanies disordering of Ca3 atoms and $P1O_4$ groups.[38] Such lattice instability relevant to Ca3 and $P1O_4$ will facilitate the reduction of $Ca_9Fe(PO_4)_7$. Ca^{2+} and Bi^{3+} ions occupying positions corresponding to the Ca3 site were also disordered at 100 K in $Ca_9Bi(VO_4)_7$, which is structurally related to β-$Ca_3(PO_4)_2$.[46]

No SHG signals were observed in centrosymmetric β' forms of $Ca_9Fe(PO_4)_7$[38] and $Ca_9In(PO_4)_7$.[47] In these two phosphates, six Fe5−O or In5−O bond lengths are all equivalent to each other, Ca3 atoms are statistically distributed between two positions near the center of symmetry, and $P1O_4$ tetrahedra are orientationally disordered. The $Fe5O_6$ octahedron is more regular in $Ca_9FeD(PO_4)_7$ than that in $Ca_9Fe(PO_4)_7$, i.e., l(Fe5−O24) = 2.088(4) Å (×3) and l(Fe5−O33) = 2.124(4) Å (×3) in $Ca_9FeD(PO_4)_7$ and l(Fe5−O24) = 1.96(3) Å (×3) and l(Fe5−O33) = 2.16(3) Å (×3) in $Ca_9Fe(PO_4)_7$.[11] As described above, the Ca3 atoms and $P1O_4$ groups have disordered arrangements in $Ca_9FeD(PO_4)_7$. The order/disorder ratio is close to unity (1.06) for Ca3 but as large as 3.50 for $P1O_4$. Nevertheless, atomic arrangements in $Ca_9FeD(PO_4)_7$ are more similar to those in β'-$Ca_9Fe(PO_4)_7$ than to those in $Ca_9Fe(PO_4)_7$,[11] which accounts for the much smaller SHG signals in $Ca_9FeD(PO_4)_7$ than those in $Ca_9Fe(PO_4)_7$.

A disordered configuration of M4 atoms was surmised in whitlockite-like materials.[8] In structure refinements of $Ca_{10}Li(PO_4)_7$,[48] $Ca_9MgLi(PO_4)_7$,[49] and $Ca_9CuLi(PO_4)_7$,[50] Li^+ ions were split into two pieces along the c-axis to be located at the M4 site. Because Li^+ ions hardly contribute to XRD intensities, we need to verify this split-atom model, resorting to neutron diffraction where b_c is −1.90 fm for Li.[33] In $Ca_9Cu_{1.5}(PO_4)_7$[51] and $Sr_{9.1}Cu_{1.4}(PO_4)_7$,[52] Cu^{2+} ions proved to split in three M4 atoms slightly off the 3-fold rotation axis. Our structure refinement of $Ca_{9.333}Fe_{1.167}(PO_4)_7$ revealed locally different locations of Ca^{2+} and Fe^{2+} ions at the M4 site: the Ca4 and Fe4 sites. During the thermal decomposition of $Ca_9FeD(PO_4)_7$ under Ar, orientation of $P1O_4$ groups alters to a certain extent. In concert with this structural change, Fe^{2+} ions migrate from the Fe5 site to the Fe4 site, and Ca^{2+} ions from the Ca1, Ca2, and/or Ca3 sites to the Ca4 site, as denoted by arrows in Figure 10a.

(46) Evans, J. S. O.; Huang, J.; Sleight, A. W. *J. Solid State Chem.* **2001**, *157*, 255.
(47) Morozov, V. A.; Belik, A. A.; Stefanovich, S. Yu.; Grebenev, V. V.; Lebedev, O. I.; Van Tendeloo, G.; Lazoryak, B. I. *J. Solid State Chem.* **2002**, *165*, 278.
(48) Morozov, V. A.; Belik, A. A.; Kotov, R. N.; Presnyakov, I. A.; Khasanov, S. S.; Lazoryak, B. I. *Crystallogr. Rep.* **2000**, *45*, 13.
(49) Morozov, V. A.; Presnyakov, I. A.; Belik, A. A.; Khasanov, S. S.; Lazoryak, B. I. *Crystallogr. Rep.* **1997**, *42*, 758.
(50) Yanov, O. V.; Morozov, V. A.; Koznyakov, I. V.; Khasanov, S. S.; Lazoryak, B. I. *Russ. J. Inorg. Chem.* **1998**, *43*, 1481.
(51) Belik, A. A.; Yanov, O. V.; Lazoryak, B. I. *Mater. Res. Bull.* **2001**, *36*, 1863.
(52) Belik, A. A.; Malakho, A. P.; Lazoryak, B. I.; Khasanov, S. S. *J. Solid State Chem.* **2002**, *163*, 121.

In the present study, we have successfully determined the crystal structure of $Ca_9FeD(PO_4)_7$ and clarified the structural differences between $Ca_9FeD(PO_4)_7$ and $Ca_9Fe(PO_4)_7$. Neutron powder diffraction was most effective in determining the locations of the D atoms. The crystal data of the two phosphates have enabled us to put forward the mechanisms of reducing $Ca_9Fe(PO_4)_7$ by D_2 (H_2) and decomposition of $Ca_9FeD(PO_4)_7$ under Ar. We will further apply TOF neutron powder diffraction to other related phosphates containing DPO_4^{2-} ions.

Acknowledgment. The authors thank S. S. Khasanov of Institute of Solid State Physics for the XRD experiments, K. V. Pokholok of Moscow State University for the measurements of the Mössbauer spectra, E. M. Kopnin of National Institute for Materials Science for the magnetic-susceptibility measurements, and A. I. Beskrovnyi of the Frank Laboratory of Neutron Physics of the JINR for preliminary neutron diffraction experiments. This work was partially supported by the Russian Foundation for Basic Research (Grants 00-03-32660 and 01-03-06122). A.A.B. acknowledges the award of the STA Fellowship from the Japan Science and Technology Corporation.

CM020411+